Section 1.4.2 Mesh Implementation for GSDT Submission

San Joaquin Renewables Class VI Permit Application AoR and Corrective Action Plan

Prepared for

San Joaquin Renewables LLC
McFarland, California

Submitted to

U.S. Environmental Protection Agency Region 9
San Francisco, California

Prepared by

DBS&A
Daniel B. Stephens & Associates, Inc.
a Geo-Logic Company

43 Randolph Road, #129
Silver Spring, Maryland 20904
www.dbstephens.com
Project # DB19.1252.SS

October 13, 2021

The injection site is relatively close to the Pond-Poso Creek fault system. The propagation of both the carbon dioxide plume and the pressure perturbation across the fault line is thus of interest and depends on whether these faults are sealing or non-sealing. As the analyses described in the narrative permit application report show, the lateral sealing effectiveness critically depends on the shale gouge ratio. Section 2.1.5.2 of the permit application report describes Allan diagrams and shale gouge ratio determination for the Pond-Poso Creek fault, and Figure 2-38 of the permit application report presents a diagram and map of fine-scaled cross-sections that were generated along the fault system.

Table 1-2 of this report presents a conceptualization of the permeability of the Pond-Poso Creek fault that was generated for the purpose of TOUGH2 modeling. Permeability of the fault gouge at each fault location was determined based on the shale gouge ratio at each location for the Olcese, Upper Vedder, and Vedder 3 units. Four subcategories were assigned to each location and geologic formation along the fault, with horizontal permeability ranging from 0.001 to 0.5 millidarcies. As discussed in Section 1.6, below, additional sensitivity analysis simulations were conducted considering both sealing and non-sealing faults.

1.4 Numerical Model Implementation

Numerical modeling implementation includes converting the geologic model grid to a numerical modeling grid, and populating the grid within initial parameter values and boundary conditions. Numerical model mesh generation, initial conditions and boundary conditions are described below.

1.4.1 Mesh Generation

The three-dimensional (3-D) mesh for the TOUGH2 simulations presented in this report was created using AMESH (Haukwa, 1998) together with pre- and post-processing scripts written in Python, that (1) process relevant site characterization information, such as geological layering and fault trace data; (2) generate the input file needed to run AMESH; and (3) perform post-processing of AMESH output. Post-processing includes, for example, assigning materials to elements and removing elements and connections that are considered outside the simulation domain. Some details regarding discretization and material assignment are given below.

Creating a 3-D, unstructured grid of Voronoi elements with AMESH requires specification of 2-D grid points in the X-Y plane, which are then repeated at multiple depths in the Z direction. Note that for simplicity, latitude, longitude, and elevation are referred to as X, Y, and Z, respectively.

For the current mesh, the X-Y grid is composed of a "background" grid, which contains radial and Cartesian components, within which fault trace grid points are embedded. The resulting X-Y grid is shown in Figure 1-1.

Specifically, the background grid contains (1) a radial portion with 24 equally spaced 15° sectors, centered around the well coordinates (X,Y) = (294,000 meters [m], 3,951,600 m), and extending outward 6 kilometers (km) with a radial spacing from 10 m up to 1,000 m; (2) a Cartesian portion (surrounding the radial portion) with 1,000 m discretization in the X and Y directions; (3) a second, coarser Cartesian portion (surrounding the first Cartesian portion) with 4,000 m discretization in the X and Y directions; and (4) thin layers of elements on the north, south, east, and west boundaries. Discretization in the Z direction is given by uniform 5 m spacing over the vertical extent of relevant geological layers (from elevations of -5,500 m to 400 m).

To accurately represent each fault in the model, grid points are placed along lines determined through interpolation of fault trace data; grid points are automatically spaced along the interpolated lines in a manner that is consistent with the background grid. Additional grid points are placed on the sides of each fault grid point (in a direction from the fault grid point that is perpendicular to the fault trace) to ensure that the fault elements are smoothly connected to each other and have the desired width. In some cases, it is necessary to manually adjust a grid point (e.g., to ensure that intersecting faults are connected appropriately). When fault grid points overlap with or are too close to background grid points, those background grid points are removed.

Figure 1-2 shows a fault embedded within the radial portion of the background grid. Figure 1-3 and Figure 1-4 demonstrate how intersecting faults are connected in the mesh. The Jasmin faults (Figure 1-4) are relatively far away from the carbon dioxide injection area and are therefore embedded in a region of the background mesh with lower resolution.

Note that faults in the model are assumed to be vertical, but they may or may not extend vertically through the entire model. That is, a "potential" fault element at a given X-Y location at one depth may be assigned fault properties, whereas another potential fault element at the same X-Y position and at a different depth may be assigned some other geological material if no fault is present at that depth based on the conceptual model.

Assignment of materials in the mesh is based on (1) a dataset that contains the elevations of the upper surfaces of the geological layers of interest (ground surface, USDW, Round Mountain, Olcese, Freeman-Jewett, multiple sand and shale layers within the Vedder formation, and

Walker) on an X-Y grid with a 200 m by 200 m resolution; and (2) fault trace data in which (a) lists of X-Y coordinates form fault traces, (b) the depth ranges over which the faults are present, and (c) fault sections that receive an additional sub-category during the assignment of fault properties (e.g., such that some parts of a fault may be treated as sealing, others as partially sealing or non-sealing).

The procedure for assigning materials to the mesh processes one column of elements at a time. Each column, which corresponds to a unique pair of X-Y coordinates, is categorized as follows: (1) a column of vertical boundary elements (on the north, south, east, or west model boundaries), (2) a column of elements that may belong to a given fault depending on the depth range over which the fault is present, (3) a column of elements that are not fault elements but are next to and share a boundary to the east or west of potential fault elements, or (4) a column of regular elements from the initial background grid (i.e., all other cases).

For each element, it is determined to which geological layer the element belongs based on its elevation Z within a column and the corresponding entry in the table of geological layer data; the identified material identifier is assigned to the element. Depending on the category of element being considered (described in the previous paragraph), and based on the geological layer determination, some elements require additional consideration.

For example, to reduce the size of the mesh and increase computational efficiency, elements are removed from the mesh if they are outside of what is considered the simulation domain, namely, if they are determined to be: (a) above the ground surface, (b) more than 50 m above the Olcese surface, (c) more than 50 m below the Walker surface; or (d) south of the curved boundary on the southern and parts of the eastern borders of the model. Cutting such elements and connections from the basic grid reduces the number of elements and connections from approximately 1,343,000 to 140,000, and from approximately 4,518,000 to 432,000, respectively.

The bounding box of the final grid is given by the following coordinate ranges: 274,000 m < Longitude < 328,600 m; 3,928,200 m < Latitude < 3,970,600 m; -5,440 masl < elevation < 345 masl. This model domain size is sufficiently large so that boundary effects are insignificant, as confirmed by the results of the analysis (see Case M in Section 1.6). The injection well is located at (X,Y) = (294,000, Y = 3,951,600).

The remaining upper-most and lower-most elements in a column are specified as top and bottom boundary materials, respectively. If the top element was the ground surface, then it receives its own ground surface boundary material instead of the “top” boundary material. If a

References

Doughty, C. A., 2013. User's guide for hysteretic capillary pressure and relative permeability functions in TOUGH2. No. LBNL-6533E. Lawrence Berkeley National Lab.(LBNL), Berkeley, CA (United States), 2013.

Doughty, C., 2010. Investigation of CO2 plume behavior for a large-scale pilot test of geologic carbon storage in a saline formation, Transp. Porous Med., 82, 49–76, 2010.

Finsterle, S., 2021. iTOUGH2-EOS1nT: A Nonisothermal Two-Phase Flow Simulator for Water and Multiple Tracers User's Guide. Finsterle GeoConsulting, Kensington CA, July, 19 2021.

Finsterle, S., Commer, M., Edmiston, J. K., Jung, Y., Kowalsky, M. B., Pau, G. S. H., ... & Zhang, Y. (2017). iTOUGH2: A multiphysics simulation-optimization framework for analyzing subsurface systems. Computers & Geosciences, 108, 8-20.

Nicot, J.-P., Oldenburg, C.M., Bryant, S.L., Hovorka, S.D., 2008. Pressure perturbations from geologic carbon sequestration: Area-of-review boundaries and borehole leakage driving forces: presented at the 9th International Conference on Greenhouse Gas Control Technologies (GHGT-9), Washington, D.C., November 16-20, 2008. GCCC Digital Publication Series #08-03h.

Pruess, K., C. Oldenburg, and G. Moridis, 2012. TOUGH2 User's Guide, Version 2.1, Report LBNL-43134, Lawrence Berkeley National Laboratory, Berkeley, Calif., 2012.

Pruess, K. (2005). ECO2N: A TOUGH2 fluid property module for mixtures of water, NaCl, and CO2 (p. 76). Berkeley, CA: Lawrence Berkeley National Laboratory.

Pruess, K., J. Garcia, T. Kovscek, C. Oldenburg, J. Rutqvist, C. Steefel, and T. Xu. 2004. Code intercomparison builds confidence in numerical simulation models for geologic disposal of CO2. Energy 29:1431–1444.

Rinaldi, A.P., V. Vilarrasa, J. Rutqvist and F. Cappa. 2015. Fault reactivation during CO2 sequestration: Effects of well orientation on seismicity and leakage. Greenhouse Gas Sci Technol. 5:645–656 (2015); DOI: 10.1002/ghg

Spycher, N., Pruess, K., & Ennis-King, J. (2003). CO2-H2O mixtures in the geological sequestration of CO2. I. Assessment and calculation of mutual solubilities from 12 to 100 C and up to 600 bar. Geochimica et cosmochimica acta, 67(16), 3015-3031.

Van Genuchten, M. T. (1980). A closed-form equation for predicting the hydraulic conductivity of unsaturated soils. Soil science society of America journal, 44(5), 892-898.

Figures

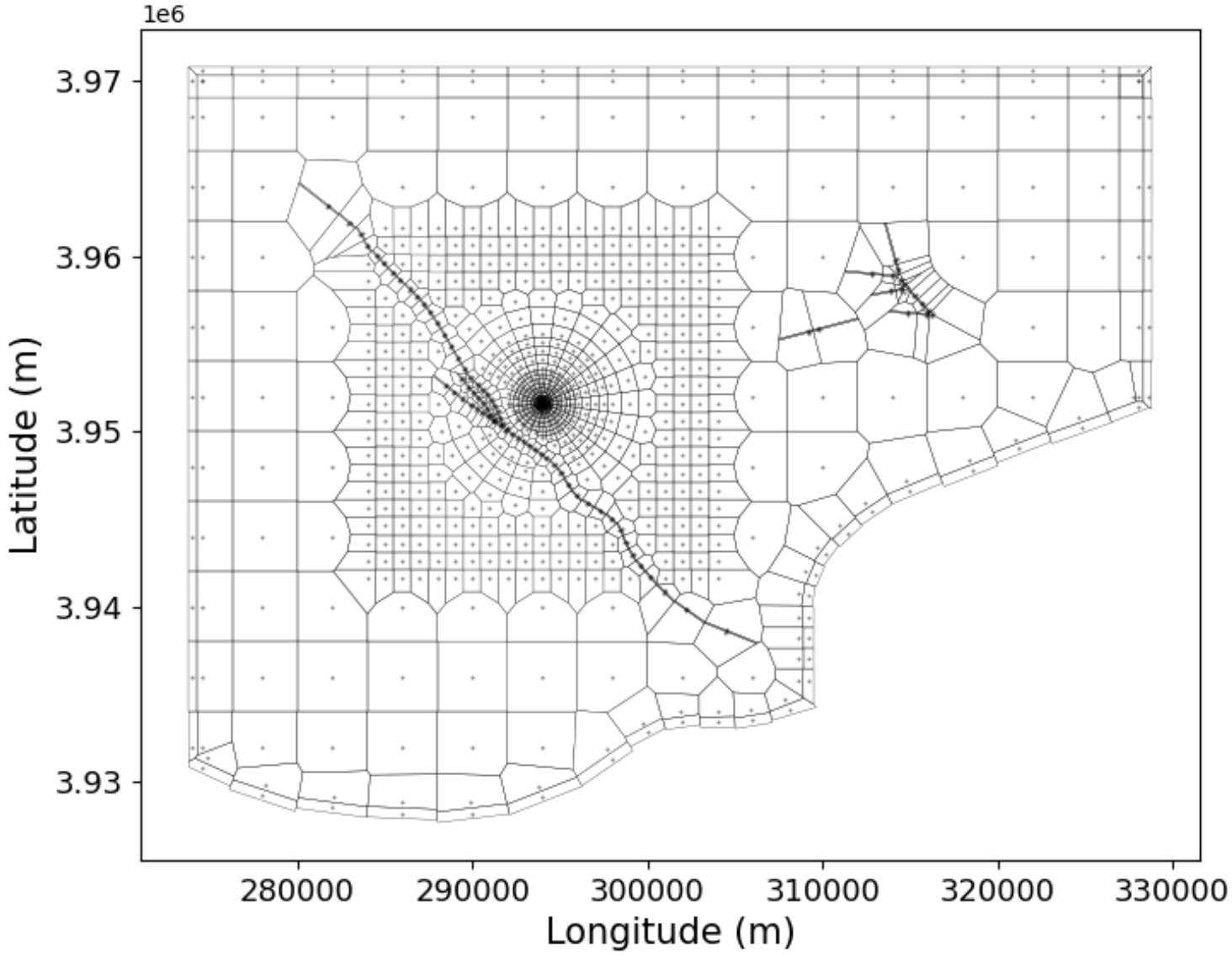

Notes: Plan view of the 3-D mesh used in the TOUGH2 simulations presented in this report, which includes faults embedded in a background mesh containing radial and Cartesian regions and thin boundary elements on the north, south, east, and west boundaries.

SAN JOAQUIN RENEWABLES

Mesh Plan View

9/14/2021 DB19.1252

Figure 1-1

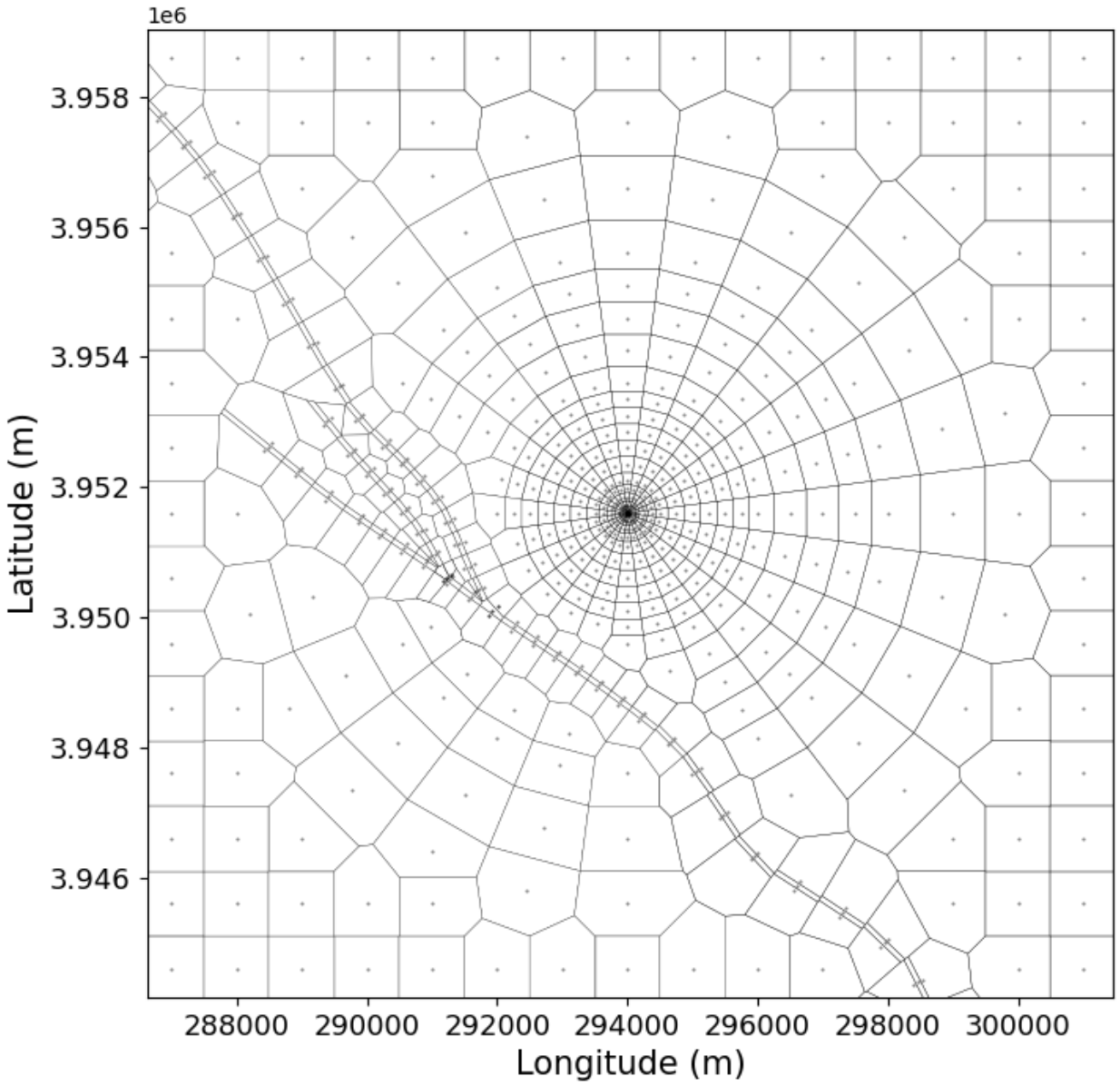

SAN JOAQUIN RENEWABLES

Mesh Expanded View, Radial Portion

9/14/2021 DB19.1252

Figure 1-2

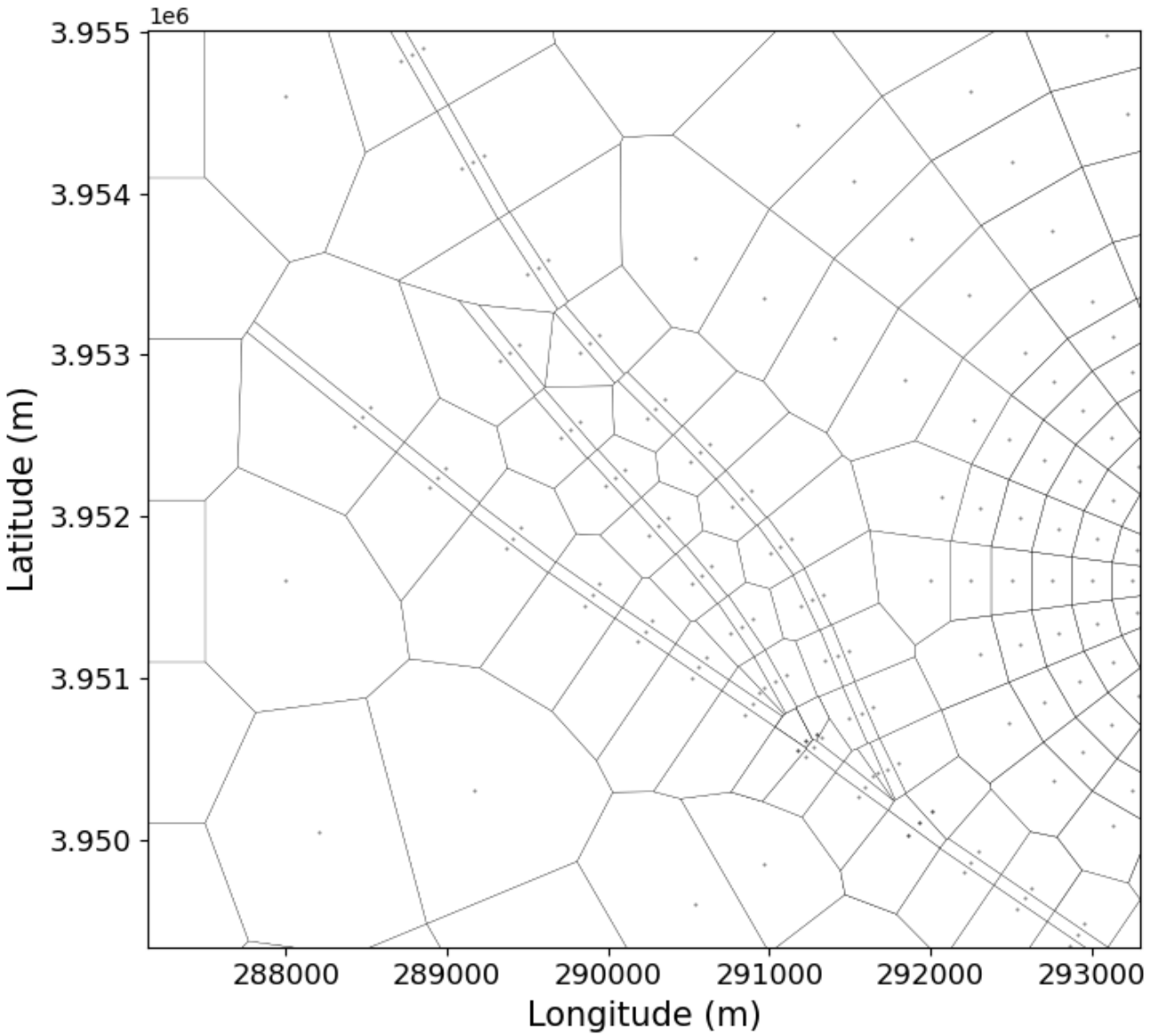

SAN JOAQUIN RENEWABLES

Mesh Enlarged View, Intersections of the Pond-Poso Creek Faults

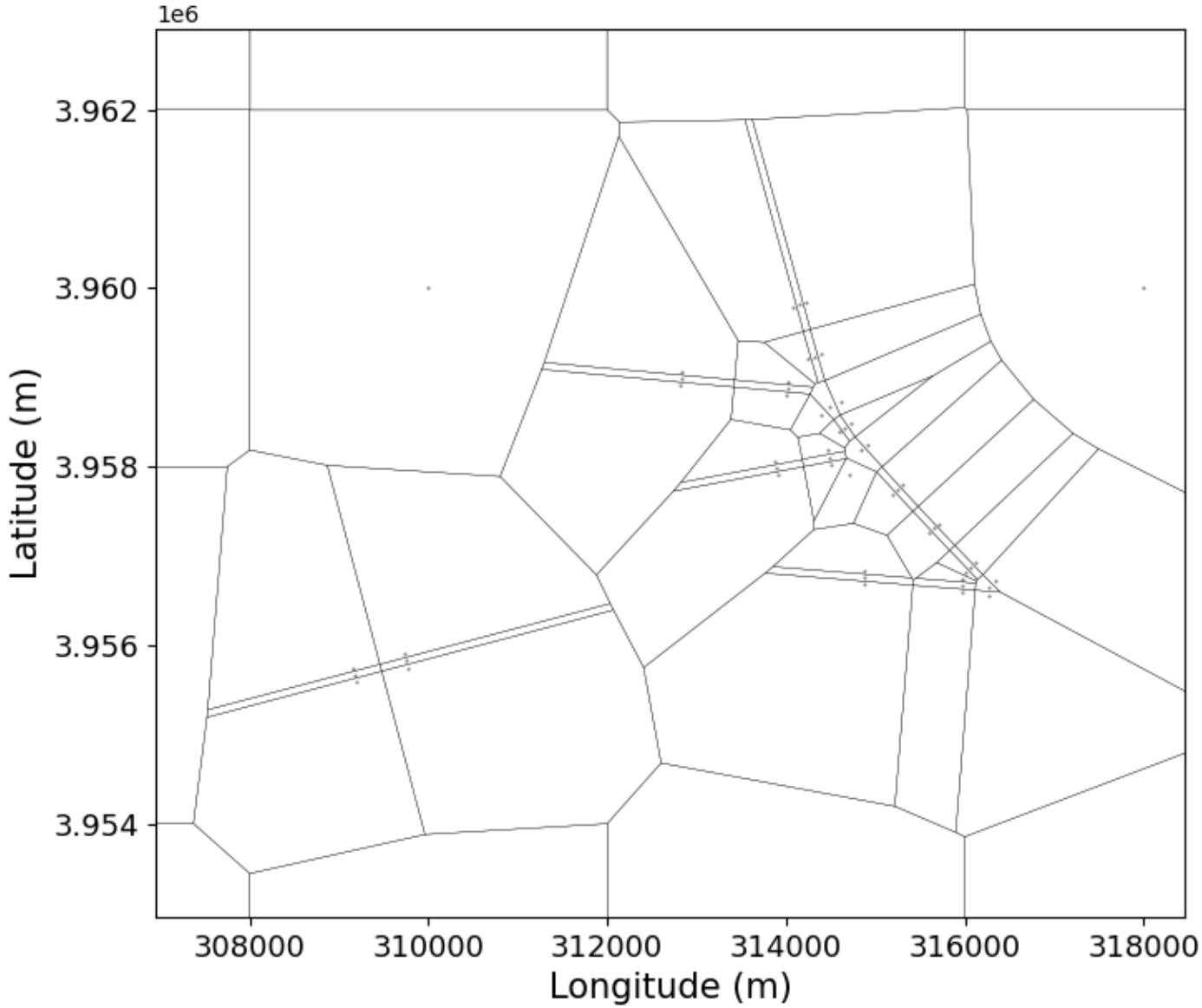

SAN JOAQUIN RENEWABLES

Mesh Enlarged View, Jasmin Fault Elements and Intersections

9/14/2021 DB19.1252

Figure 1-4

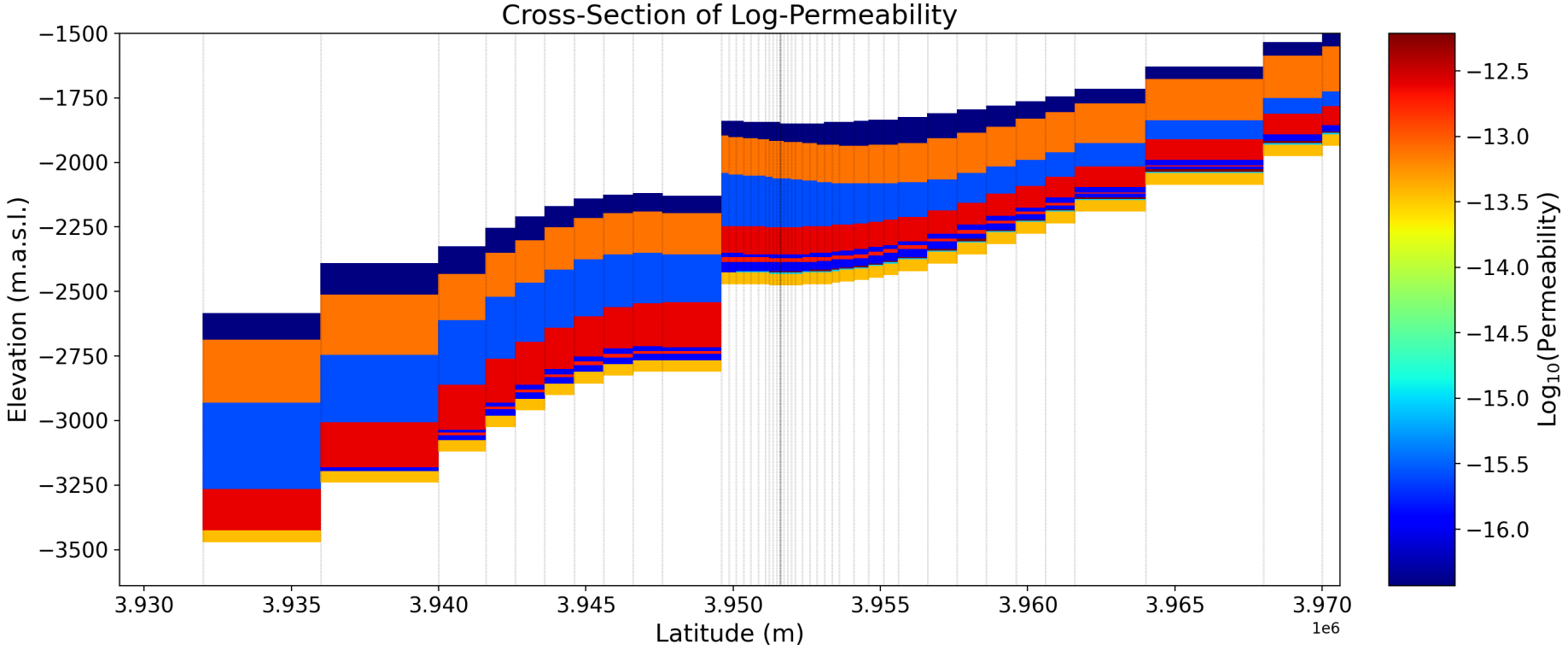

SAN JOAQUIN RENEWABLES

Permeability Cross Section Through the Injection Well from South to North

9/14/2021 DB19.1252

Figure 1-5